Supporting information for: Through-Bond Interactions and the Localization of Excited State Dynamics

Oliver Schalk, Andrey E. Boguslavskiy, Albert Stolow*, and Michael S. Schuurman*

Steacie Institute for Molecular Sciences, National Research Council of Canada, Ottawa, Ontario K1A 0R6, Canada

E-mail: albert.stolow@nrc.ca,michael.schuurman@nrc.ca

Ground State Processes

As far as the ground state dynamical processes are concerned, the TRPES-spectra of CHE and CHD are clearly different on a ps-time scale. This indicates that different product channels are open for the two molecules. In addition, some of the products following CHD photoexcitation are likely resonant with the probe pulse, leading to an increased yield of photoelectron signal. As discussed in the following section, different rise times are seen in different energy regions (Figure 3 b) indicating different dynamics and joint to the variety of products found in the liquid phase (vide infra). In the gas phase the final product of CHD photodissociation is benzene, following loss of two H-atoms or an H_2 molecule,[1,2] likely occurring within 2-3 ns after excitation at 212 nm.[3] Here, we observe, that the slowest rise of the TRPES-spectrum occurs with a time constant of several

*To whom correspondence should be addressed

hundreds of ps, agreeing with previous measurements and RRKM calculations (however, using a somewhat lower total energy than in our experiments).

In liquid phase, energy is readily dissipated into the surrounding solvent, thereby "cooling" the vibrationally hot molecules after passage through the intersection. This stabilizes the geometrical structures that achieve the ground state. In CHE, five products were observed[4–6] (see Figure 1): CHE itself, the retro Diels-Alder products, methylenecyclopentane (MCP), and bicyclo[3,1,0]hexane (BH). The easiest product to assign is CHE which directly follows the [1,3] H-shift. Each of the other reaction paths ends in a carbene ground state structure[7] which is reactive enough to undergo further rearrangements in the ground state on a ps-time scale, even in the liquid phase. Especially the cleavage channels are leading to ring contraction. The topography of the intersection corresponding to α-cleavage, for example, clearly shows that motion along one of the branching space coordinates, the **g**-direction as shown in Figure 2 in the paper (P2), results in ring closure to form a five-membered cyclopentane ring, with a single CH substituent. However, based on the concerted motion of the terminal CH group relative to ring to closure, a secondary hydrogen shift from the ring to the substitutent group is also possible. The **h**-direction for this species involves the rotation of the now-opened ring to a *trans*-orientation.

The minimum energy crossing point associated with β-bond cleavage is qualitatively similar to the α-cleavage intersection. The **g**-direction again corresponds to ring-closure, this time yielding a diradical species with a singlet coupled pair of electrons; one on the CH_2 substituent and another on the carbon at the 2-position in the five-membered ring. The **h**-direction corresponds to ring opening motion, suggesting that this product channel may be assisted by favorable gradients on the excited S_1 surface. As with the previous bond-cleavage cases, significant electron density is observed between the two carbons involved in ring closure identifying this motion as an accessible product channel.

As Figure P2 evinces, the **g**-direction for the bond cleavage intersection in CHD is again associated with ring-closure, while the **h**-direction is identified with rotation about the carbon-carbon single bond. In this case, ring closure would leave the π-system of the second carbon-carbon dou-

ble bond intact, yielding a cyclopentene species with a CH substituent. These orbitals demonstrate that significant σ-bonding electron density remains between carbons at the 1- and 5-positions, suggesting that a ring closure pathway is at least energetically accessible.

Photoelectron spectra

In order to extract time constants for the underlying processes which allow a direct comparison of CHE and CHD, photoelectron spectra were cut into energy slices of $\Delta E \approx 0.04$ eV and these were fit according to

$$S(E,\Delta t) = \sum_i A_i(E) \cdot P_i(\Delta t) \otimes g(\Delta t) \tag{1}$$

where $A_i(t)$ is the decay associated photoelectron spectrum of the ith slice, which has a time dependent population $P_i(\Delta t)$, and $g(\Delta t)$ is the experimentally determined Gaussian cross-correlation function. For each molecule, the spectrum was initially divided into different regions that were analyzed separately (see Figures P4 and P5 and Figure 2, where three slices through the spectrum are shown together with the contribution of the different processes according to the time constants shown in Table 1 of the paper). Region II contains the initial dynamics, originating at $\Delta t = 0$, was considered first, followed by analysis of the time-delayed signals.

As discussed in Ref. 8, the representation of the TRPES data by Eq. (1) works best for rigid molecules. In contrast, large amplitude motions in the excited state will evolve the photoelectron spectrum due to changing Franck-Condon spectra between the excited state and the ionic state. In such a case, the decay times τ_i cannot be uniquely associated with changes in the electronic character of the excited state wavepackets. One approach that can yield additional information about the dynamics involves varying the 'time zero' of the fitting routine which, although unphysical, can serve as a measure to quantify the timescales of molecular rearrangements.

The ionization potentials of CHE and CHD are 8.94 eV and 8.82 eV, respectively, and therefore the energetic cut-off for a one photon pump, one photon probe experiment (subsequently denoted

a [1,1']-process) lies at 10.85 eV - IP $\approx$ 2 eV for both molecules. The first excited ionic state (D_1) of CHE appears at 10.7 eV and can just be reached by a [1,1']-process, whereas for CHD, the D_1-state lies at 9.88 eV,[9] about 1 eV below the energy cut-off. The second excited ionic state (D_2) of CHD lies at 11.0 eV and cannot be reached by a [1,1']-process. Photoelectrons with kinetic energies more than 2 eV are due to [1,2']-processes having a total photon energy of 15.5 eV.

Cyclohexene (CHE)

As Figure P5 evinces, five regions can be distinguished in the CHE TRPES spectrum: Between 1.8 and 2.0 eV (denoted region II), a nearly Gaussian band can be observed with a decay constant of $\tau_1^{CHE} = (40 \pm 10)$ fs. With a decreased count rate, a second time constant $\tau_5^{CHE} = (500 \pm 50)$ fs can be further identified. Table 1 in the paper gives an overview of the extracted CHE time constants. Finally, we note that the signal slightly rises after 300 ps. This rise can be seen throughout the entire spectrum and cannot be isolated in a single region. In Figure 3 a), we show the time evolution of this long time component at delay times of 10, 100, 300 and 900 ps. This spectrum does not rise uniformly, but rather displays a "red shift" toward lower electron kinetic energy. This long time signl we believe is most likely due to dynamic rearrangements of the hot ground state molecule (see discussion part in the paper). Overall, the decay spectrum of this long time component is very weak, barely 5% of the main peak in region I.

The spectrum between 0.6 and 1.6 eV (region I) rises with the cross correlation but is delayed from that of region II by (30 ± 10) fs ($\approx \tau_1^{CHE}$). The spectrum decays biexponentially with $\tau_2^{CHE} = (40 \pm 10)$ fs and τ_5^{CHE}. However, due to large amplitude motion, the value of τ_4 varies between 500 fs and 2 ps over the whole region and no unique value can be assigned to this time constant (see discussion). Moreover, a slight shift in the spectrum toward slower rise times for the lower kinetic electron energies can be recognized (from 20 to 50 fs), again indicating large amplitude excited state motions (see above and the discussion section in the paper).

In the region between 2.0 and 2.35 eV (region III), the rise is delayed by an additional 60 fs ($\approx \tau_2$), as compared with region I. Since two probe photons are required to generate photoelectrons

with this kinetic energy (subsequently denoted a [1,2']-process), the cross correlation is reduced to 120 fs. The signal is much weaker than the signal below 2.0 eV, and decays biexponetially with $\tau_3^{CHE} = (175 \pm 50)$ fs and $\tau_6^{CHE}(5 \pm 1.5)$ ps. A strong [1,2']-signal is also observed between 3.35 and 3.85 eV (region IV). It rises with the same time constant as the signal in region III, but decays significantly faster, with time constants of $\tau_4^{CHE} = (60 \pm 15)$ fs and τ_6^{CHE}. The region between region III and region IV is dominated by a so-called "bleaching signal" (i.e. when, due to ground state depletion, more photoelectrons are generated by pump and/or probe pulse alone than by both pulses), which co-adds with the pump-probe signal. Since it is unclear how to disentangle these two processes, no analysis of this region was attempted.

Cyclohexa-1,4-diene (CHD)

The spectrum of CHD is shown in Figure P6 and can likewise be divided into energy regions, as was the case for CHE. Region II (1.86 - 2.1 eV) appears delayed by 20 fs with respect to the independently measured t_0. This delayed rise has some minor implications. Probably, the Rydberg state signature is overlapped with the signature of the $\pi\pi^*$-state which leads to an apparent delay in the fitting routine. Moreover, it is possible that some excitation is to the dark $\pi\pi^*$-state, although the molecule is rigid and deformations from D_{2h}-symmetry should be small. The signal then decays biexponentially with $\tau_1^{CHD} = (65 \pm 15)$ fs with a small contribution of $\tau_5^{CHD} = (1.3 \pm 0.4)$ ps. As in CHE, a long time constant between 150 and 500 ps can be found throughout the whole spectrum (see Figure 3 b)). The amplitude of this slowly rising component is significantly greater than the analogous component in CHE. We speculate that this might be explained by the generation of hot ground state benzene[3] which is resonant with the probe photon and would have, therefore, increased photoionization probability. Absent in the CHE experiment, benzene formed by photodissociation of CHD could resonantly absorb probe photons (the origin of the UV-spectrum is at 259 nm, however, the product molecule in the gaseous phase is vibrationally very hot and its spectrum is heavily red-shifted, see, e.g. Ref. 10). However, transient ground state species other than benzene could also be formed following CHD's return to the ground state, one of them possibly

being cyclohexa-1,3-diene, as this may also be resonantly ionized by the probe pulse.

The linear shift of the spectrum in region I varies between rise times of 20 to 80 fs over the range 1.8 to 0.6 eV, and this effect is more pronounced than in CHE. The spectrum can be fit by a biexponential decay with $\tau_2^{CHD} = (50 \pm 15)$ fs and τ_5 in addition to the ps-rise.

Region III between 2.2 and 2.6 eV is delayed by 120 fs with respect to t_0 and decays with $\tau_3 = (60 \pm 10)$ fs and $\tau_6^{CHD} = 1.6 \pm 0.3$ ps. The final rise time in this region is ≈ 50 ps, significantly faster than in other regions as can be seen, e.g., in Figure 3 b). At higher kinetic energies, a "bleach" region is again observed where the signal changes from negative to positive within 50 fs. This "bleach" influences the signal in region III, since the rise is clearly faster than the cross correlation.

Region IV is on the high energy side of the partial bleach region. The band is shifted by 100 fs and the decay constants are $\tau_3^{CHD} = (60 \pm 10)$ fs and τ_6^{CHD}. Both the time shift and time constants agree with those found in region III, when the fact that the signal is modified by a bleach component at small delay times is taken into account.

Orbital and geometric parameter information

The following Figures and Tables contain orbital and geometric parameter information. Figure 4 provides additional orbital plots for the terminal points on each interpolated path, for CHE and CHD, respectively, and Figure 5 displays the energy of the low-lying cationic electronic states, relative to the corresponding ground state minimum energy. What follows in Tables 1 to 11 are the Cartesian coordinates (Angstrom) and absolute energies (in hartrees) for the optimized end points for each interpolated paths. Tables 1 and 2 are the optimized ground state minima for CHE and CHD, respectively, and were the starting points for each path. Tables 3 to 11 evince the Cartesian geometries of the minimum energy conical intersections that serve as the end point for each path.

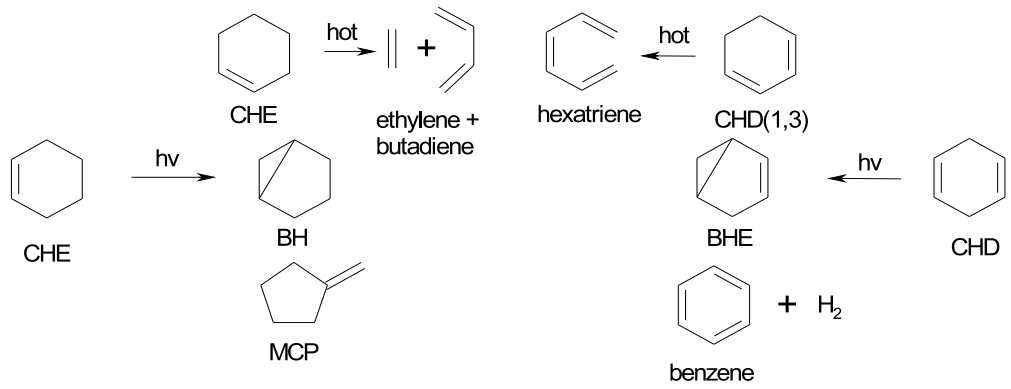

Figure 1: Possible reactions of cyclohexene and cyclohexadiene upon photoexcitation. See text for details.

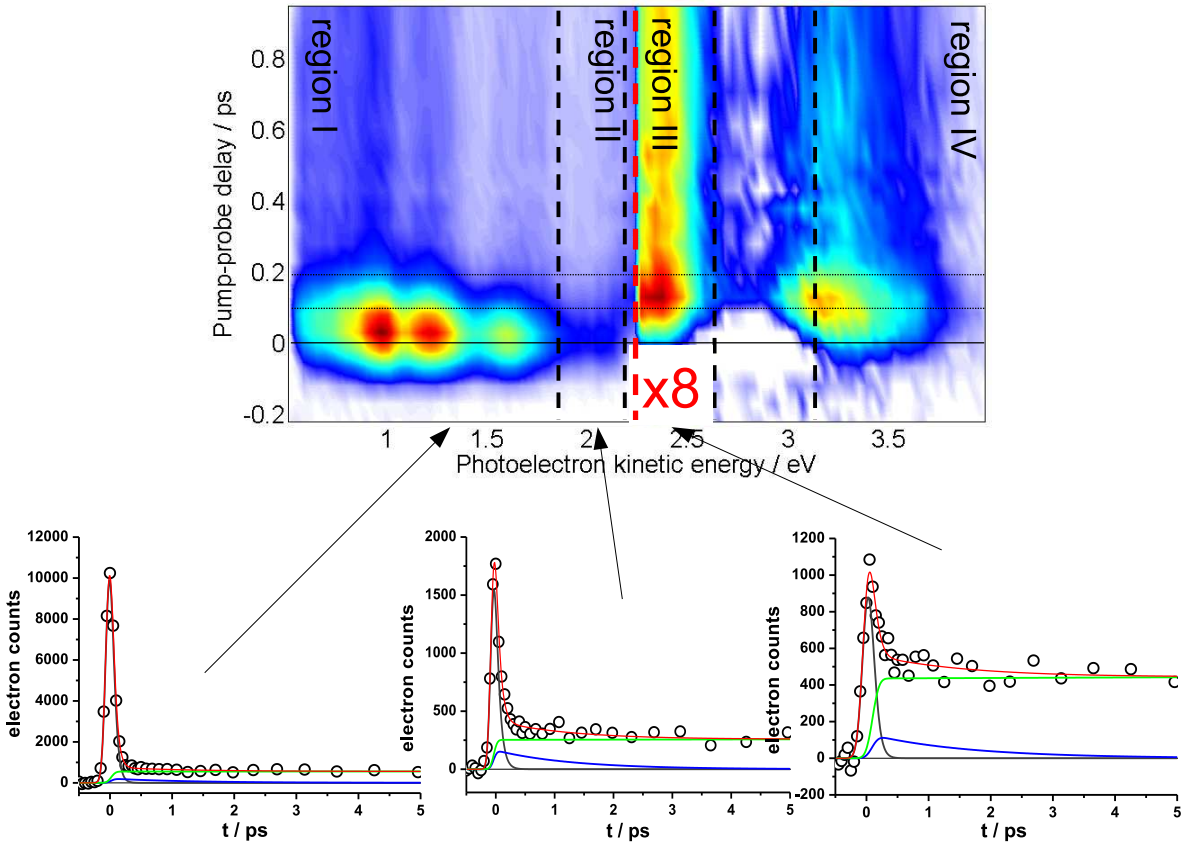

Figure 2: Photoelectron spectrum of CHD as shown in the main manuscript. Added are data slices at 1.3, 1.9 and 2.2 eV together with the results of the global fitting (see Table 1 of the manuscript). The different lines represent the decay according to τ_1 (gray), τ_2 (blue) and the long time constant (green). The total fit is indicated by the red line.

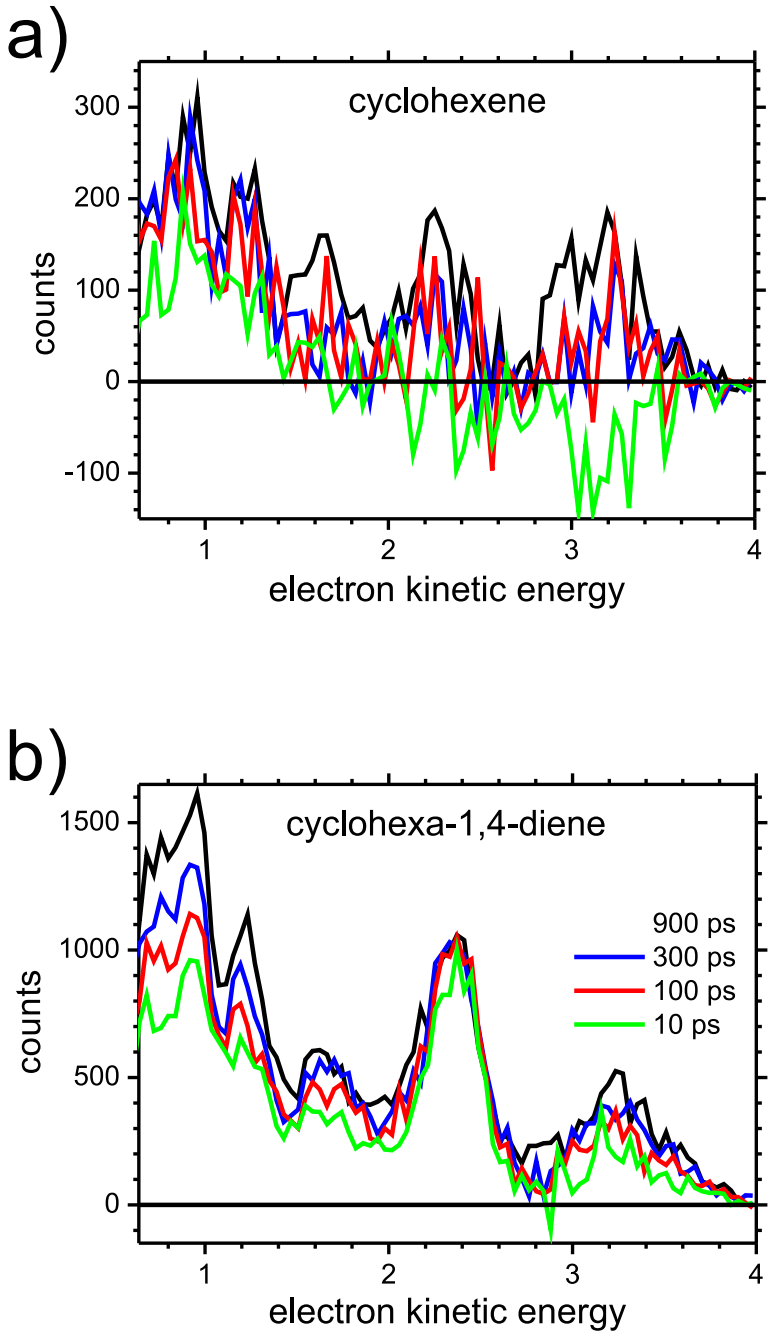

Figure 3: Photoelectron spectra of a) cyclohexene and b) cyclohexadiene at a pump wavelength of $\lambda_p = 200$ nm and a probe wavelength of $\lambda_e = 267$ nm at delay times of 10 (green), 100 (blue), 300 (red) and 900 ps (black).

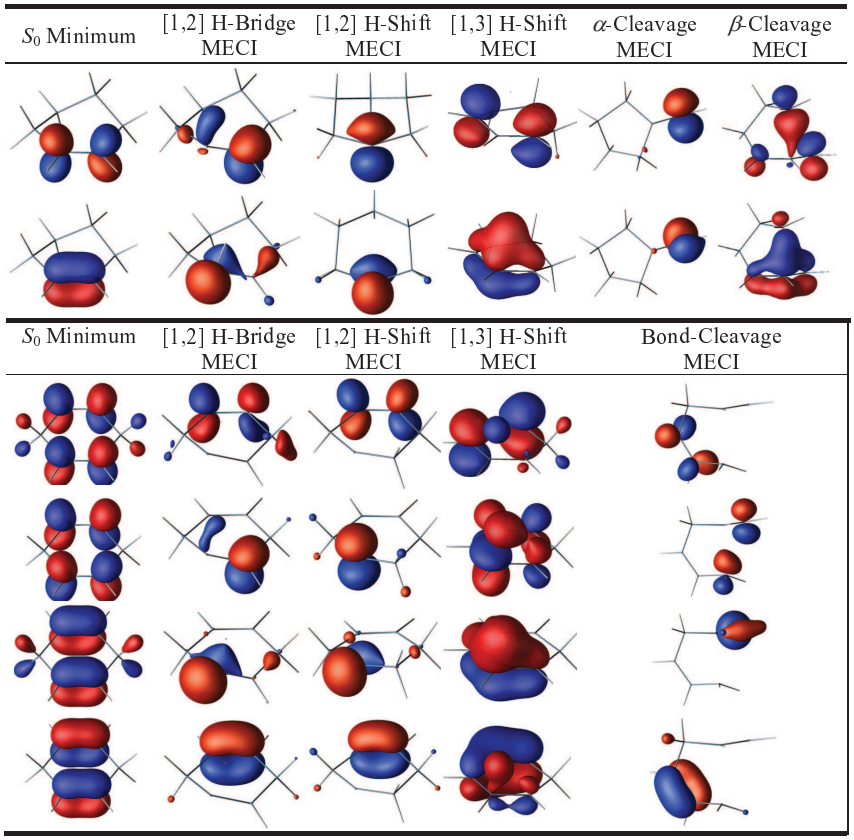

Figure 4: Molecular orbitals at the terminal points on the linearly interpolated paths between the Franck-Condon point and the [1,2]-hydrogen bridge, [1,2]-hydrogen shift, [1,3]-hydrogen shift, α- and β-bond cleavage (CHE, top two rows), and single-bond cleavage (CHD, bottom four rows) S0/S1 conical intersections.

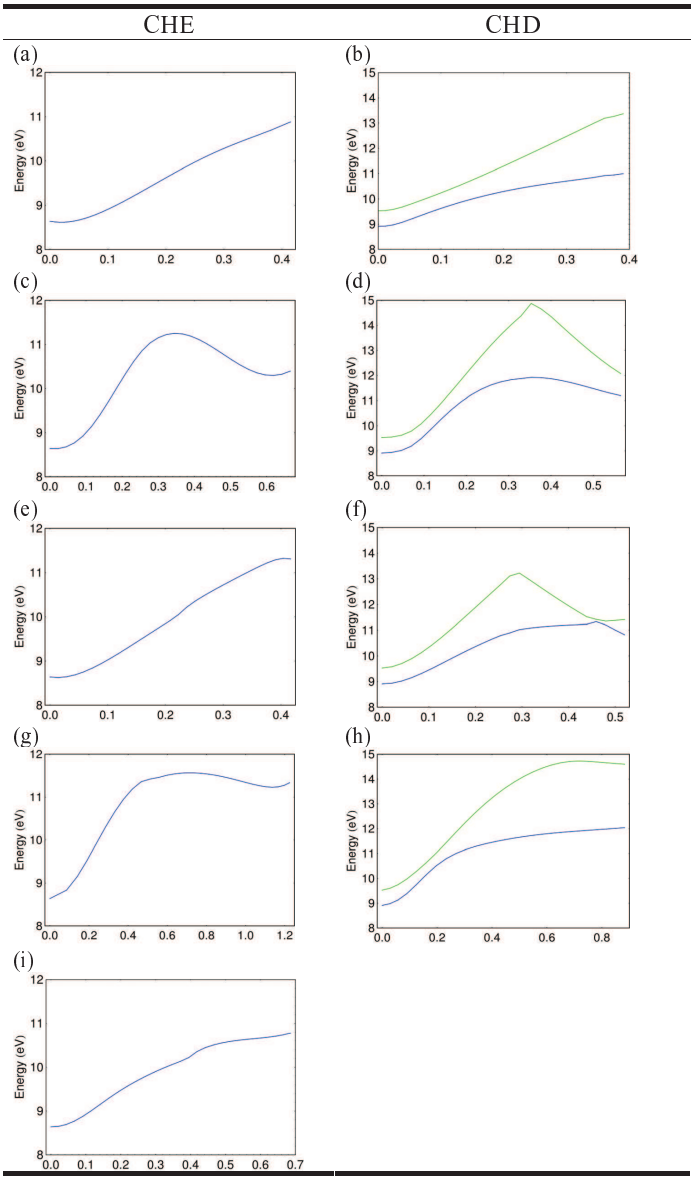

Figure 5: Cationic D_0 (blue) and D_1 (green, for CHD only) energies at points along the paths shown in panels (a)-(i) in Figure 3 in the main body of the text .

Table 1: CHE Minimum Energy Structure

S_0 Energy: -233.7782236933			
C	0.128412	-0.662338	0.059943
C	-0.128412	0.662338	0.059943
C	0.180869	-1.498629	1.319408
C	-0.180869	1.498629	1.319408
C	0.307106	0.700850	2.534485
C	-0.307106	-0.700850	2.534485
H	0.224254	-1.183616	-0.891765
H	-0.224254	1.183616	-0.891765
H	0.443296	2.393838	1.184786
H	-0.443297	-2.393838	1.184786
H	1.201183	-1.861017	1.486680
H	-1.201183	1.861017	1.486680
H	1.399652	0.609629	2.491281
H	-1.399651	-0.609629	2.491282
H	0.063010	1.234636	3.459765
H	-0.063010	-1.234636	3.459765

Table 2: CHD Minimum Energy Structure

S_0 Energy: -232.5794601184			
C	0.674447	1.254120	0.000000
C	-0.674447	1.254120	0.000000
C	0.674447	-1.254120	0.000000
C	-0.674447	-1.254120	0.000000
C	1.511201	-0.000000	0.000000
C	-1.511200	0.000000	0.000000
H	1.205614	2.205455	0.000000
H	-1.205614	2.205455	0.000000
H	1.205614	-2.205455	0.000000
H	-1.205614	-2.205455	0.000000
H	2.175786	0.000000	0.875449
H	2.175786	0.000000	-0.875449
H	-2.175786	0.000000	0.875449
H	-2.175786	0.000000	-0.875449

Table 3: CHE Minimum Energy [1,2] H-Bridge S_0-S_1 Conical Intersection

S_0,S_1 Energies: -233.587270223545, -233.587264318002			
C	0.297951	-0.594325	0.000076
C	-0.254497	0.691770	0.061232
C	0.113280	-1.482531	1.259945
C	-0.213278	1.535604	1.312838
C	0.321845	0.732547	2.502545
C	-0.304210	-0.668323	2.507856
H	1.266630	-0.063907	0.324757
H	-0.697497	1.191718	-0.814325
H	0.346911	2.465139	1.139659
H	-0.645821	-2.242967	1.046797
H	1.048930	-2.016643	1.449862
H	-1.257512	1.840686	1.484843
H	1.413276	0.648282	2.432815
H	-1.396173	-0.552292	2.508961
H	0.103001	1.266038	3.433452
H	-0.038081	-1.204778	3.425923

Table 4: CHE Minimum Energy [1,2] H-Shift S_0-S_1 Conical Intersection

S_0,S_1 Energies: -233.607732565977, -233.607683618835			
C	-0.103183	-0.541033	-0.172170
C	-0.076896	0.845138	0.253907
C	0.145361	-1.346401	1.143063
C	0.060078	1.704841	1.424682
C	0.275776	0.702833	2.608495
C	-0.426312	-0.642837	2.380595
H	0.673295	-0.806600	-0.897833
H	-1.067893	-0.837061	-0.607935
H	0.915882	2.394189	1.386997
H	-0.288612	-2.345668	1.028130
H	1.226290	-1.463766	1.276856
H	-0.838996	2.314556	1.617042
H	1.351375	0.519605	2.712963
H	-1.507299	-0.491457	2.263243
H	-0.075153	1.173688	3.533463
H	-0.279109	-1.280452	3.261139

Table 5: CHE Minimum Energy [1,3] H-Shift S_0-S_1 Conical Intersection

S_0,S_1 Energies: -233.553747148746, -233.553711123969			
C	-0.064027	-0.780898	0.130568
C	0.159725	0.603313	0.083100
C	-0.253372	-1.478108	1.331947
C	-0.115414	1.427318	1.308288
C	0.231078	0.662131	2.594741
C	-0.384262	-0.744561	2.640301
H	0.087310	-1.362535	-0.778009
H	0.434163	1.075004	-0.854840
H	0.438376	2.371083	1.275826
H	-0.427564	-2.550043	1.309310
H	1.529374	-0.816167	0.628752
H	-1.185242	1.690047	1.327620
H	1.320971	0.563460	2.646315
H	-1.454066	-0.672506	2.891854
H	-0.086123	1.235527	3.471516
H	0.078957	-1.324828	3.446479

Table 6: CHE Minimum Energy α-cleavage S_0-S_1 Conical Intersection

S_0,S_1 Energies: -233.601229848548, -233.601210881490			
C	-0.114924	0.027819	0.373790
C	0.740807	0.257623	-0.782049
C	0.262669	-1.201295	1.251022
C	-0.262921	1.218192	1.384638
C	0.145899	0.651284	2.754064
C	-0.225519	-0.833274	2.655030
H	-1.106885	-0.166304	-0.081341
H	0.933471	0.350805	-1.839494
H	0.345078	2.073554	1.083444
H	-0.164920	-2.125744	0.854015
H	1.352254	-1.309373	1.261061
H	-1.308022	1.542641	1.406508
H	1.230462	0.741651	2.887213
H	-1.315138	-0.949010	2.719541
H	-0.338513	1.168123	3.588023
H	0.226757	-1.448066	3.439508

Table 7: CHE Minimum Energy β-cleavage S_0-S_1 Conical Intersection

S_0,S_1 Energies: -233.549264376487, -233.549258230238			
C	0.272210	-0.605974	0.181235
C	0.197900	0.820341	0.401629
C	-0.284386	-1.455692	1.268701
C	-0.941002	1.494136	0.804997
C	0.725975	0.572666	2.412808
C	0.005642	-0.729179	2.639868
H	0.962665	-0.999651	-0.556020
H	0.998818	1.435354	-0.015166
H	-0.942127	2.575960	0.894402
H	-1.372799	-1.600812	1.194295
H	0.163831	-2.453280	1.243368
H	-1.819456	0.950016	1.134709
H	1.777472	0.520190	2.132874
H	-0.930776	-0.535389	3.170120
H	0.492046	1.401774	3.078441
H	0.603862	-1.395082	3.272677

Table 8: CHD Minimum Energy [1,2] H-Bridge S_0-S_1 Conical Intersection

S_0,S_1 Energies: -232.383323660372, -232.383313304147			
C	0.139420	0.698286	1.302557
C	-0.175957	-0.685831	1.270677
C	-0.010526	0.676748	-1.223073
C	0.049437	-0.660988	-1.221216
C	-0.034713	1.530693	0.028676
C	-0.007230	-1.521541	0.025000
H	1.273123	0.247550	0.996189
H	-0.508671	-1.218496	2.169221
H	-0.033192	1.195458	-2.182973
H	0.090430	-1.191541	-2.172038
H	0.743211	2.296898	-0.033282
H	-0.990829	2.071461	0.081529
H	0.875899	-2.175761	0.087682
H	-0.867690	-2.203787	-0.026429

Table 9: CHD Minimum Energy [1,2] H-Shift S_0-S_1 Conical Intersection

S_0,S_1 Energies: -232.383720293020, -232.383654467806 Energy:			
C	-0.107257	0.872278	1.044106
C	0.029800	-0.498205	1.507083
C	-0.055962	0.723961	-1.290748
C	0.079575	-0.594040	-1.126090
C	-0.178280	1.718385	-0.139071
C	0.138011	-1.347206	0.182476
H	0.929181	-0.678484	2.119607
H	-0.829818	-0.863035	2.094010
H	-0.084841	1.148340	-2.292680
H	0.158879	-1.218014	-2.017038
H	0.636882	2.459038	-0.224997
H	-1.126827	2.273330	-0.252024
H	1.077478	-1.910672	0.211292
H	-0.666206	-2.091641	0.184860

Table 10: CHD Minimum Energy [1,3] H-Shift S_0-S_1 Conical Intersection

S_0,S_1 Energies: -232.387358229227, -232.387339421751			
C	-0.016662	0.863103	1.043090
C	0.081914	-0.521615	1.170767
C	-0.380670	0.674815	-1.358143
C	-0.002653	-0.673791	-1.327909
C	-0.473767	1.437025	-0.190735
C	0.073964	-1.410388	-0.022978
H	-0.062829	1.458175	1.952262
H	0.248105	-0.961333	2.152929
H	-0.593961	1.141452	-2.317787
H	0.104312	-1.244052	-2.244955
H	1.528009	0.672915	1.023273
H	-0.748940	2.484966	-0.220337
H	0.940517	-2.081271	0.020284
H	-0.807128	-2.072748	0.092145

Table 11: CHD Minimum Energy single-bond cleavage S_0-S_1 Conical Intersection

S_0,S_1 Energies: -232.371729297495, -232.371649823924			
C	-0.124466	0.665652	1.398098
C	0.082632	-0.659811	1.318482
C	1.181718	0.189633	-1.594273
C	0.000088	-0.384411	-1.166348
C	-0.488841	1.454164	0.194538
C	-0.054968	-1.369759	-0.009887
H	-0.028222	1.182279	2.355340
H	0.280156	-1.254560	2.209989
H	1.237903	0.737146	-2.541432
H	-0.912350	-0.273432	-1.761502
H	0.122703	2.308655	-0.087674
H	-1.538952	1.517078	-0.087587
H	0.740259	-2.113582	-0.128104
H	-1.010002	-1.910899	-0.027904

References

(1) Srinivasan, R.; White, L. S.; Rossi, A. R.; Epling, G. A. *J. Am. Chem. Soc.* **1981**, *103*, 7299.

(2) Zhao, X.; Continetti, R. E.; Yokoyama, A.; Hintsa, E. J.; Lee, Y. T. *J. Chem. Phys.* **1989**, *91*, 4118.

(3) Cromwell, E. F.; Liu, D.-J.; Vrakking, M. J. J.; Kung, A. H.; Lee, Y. T. *J. Chem. Phys.* **1991**, *95*, 297.

(4) Inoue, Y. I.; Takamaku, S.; Sakurai, H. J. *J. Chem. Soc. Perkin Trans.* **1977**, *2*, 1635.

(5) Collin, G. J.; Deslauriers, H. *Can. J. Chem.* **1983**, *61*, 1970.

(6) Collin, G. J.; Deslauriers, H.; Makulski, W. *J. Photochem.* **1987**, *39*, 1.

(7) Wilsey, S.; Houk, K. N. *J. Am. Chem. Soc.* **2002**, *124*, 11182.

(8) Schalk, O.; Boguslavskiy, A. E.; Stolow, A. *J. Phys. Chem. A* **2010**, *114*, 4058.

(9) Bieri, G.; Burger, F.; Heilbronner, E.; Meier, J. P. *Helv. Chim. Acta* **1977**, *60*, 2213.

(10) Hippler, H.; Troe, J.; Wendelken, H. J. *J. Chem. Phys.* **1983**, *78*, 5351.